Dynamic Testing Techniques for Qualifying Mars Exploration Rover Equipment to Quasi-static Landing Loads

Gregory L. Davis Ph.D.
Jet Propulsion Laboratory, California Institute of Technology

Terry D. Scharton Ph.D.
Jet Propulsion Laboratory, California Institute of Technology

Wan B. Tsoi
Jet Propulsion Laboratory, California Institute of Technology

Keywords: quasi-static load, limit load, static testing, sine pulse, electrodynamic shaker

ABSTRACT: In mid 2003, the National Aeronautics and Space Administration (NASA) will launch identical spacecraft to deliver two large rovers to the Martian surface. As with the successful *Mars Pathfinder* (MPF) mission, the *Mars Exploration Rover* (MER) spacecraft will use an airbag landing system to safely deliver its payload. Measurements from both the actual MPF landing event and high-fidelity drop testing have bounded this landing environment as an approximately 30 g excitation with a main energy lobe below 10 Hz. Because this excitation lies outside the usual range of the traditionally tested for launch environments, supplemental testing is required to fully qualify MER equipment. Since the predominant frequency of this landing excitation occurs well below the fundamental modes of the landed structure, testing approaches treating this environment as a quasi-static event may be effectively employed. A novel approach utilizing sine-burst excitations from an electrodynamic shaker is considered. This approach offers the advantages of being logistically simpler than centrifuge testing and more comprehensive than localized pull testing. In this technique, a low frequency, sine wave excitation—either a multi-cycle sine ramp or a half-sine pulse with a negative pre- and post-pulse—are input to the test article. Force gages at the shaker-test article interface measure the response, thereby determining the acceleration of the test article at its center of mass. Additionally, accelerometers at key test article locations are used to measure other critical hardware responses. These data can be subsequently incorporated into a finite element model to predict responses at other test article locations, or be extrapolated to predict responses for other similar structures.

1 BACKGROUND

In mid 2003, the National Aeronautics and Space Administration's (NASA) Jet Propulsion Laboratory (JPL) will launch identical spacecraft to deliver two large rovers to the Martian surface. As with the successful *Mars Pathfinder* (MPF) mission, the *Mars Exploration Rover* (MER) spacecraft will use an airbag landing system to safely deliver its payload. As shown in Fig. 1, MER will use a complex entry, descent, and landing (EDL) sequence involving a combination of atmospheric drag, a parachute, and retrorockets to stop the lander's descent approximately 15 meters above the Martian surface. In the terminal phase of this sequence, four airbags—one attached to each face of the tetrahedral lander—will be deployed and inflated. The airbags are designed to mitigate the inertial impact forces associated with the lander's subsequent free fall. After as many as 10 bounces, the lander will come to a rolling stop, thereby enabling the deployment of the roving payload.

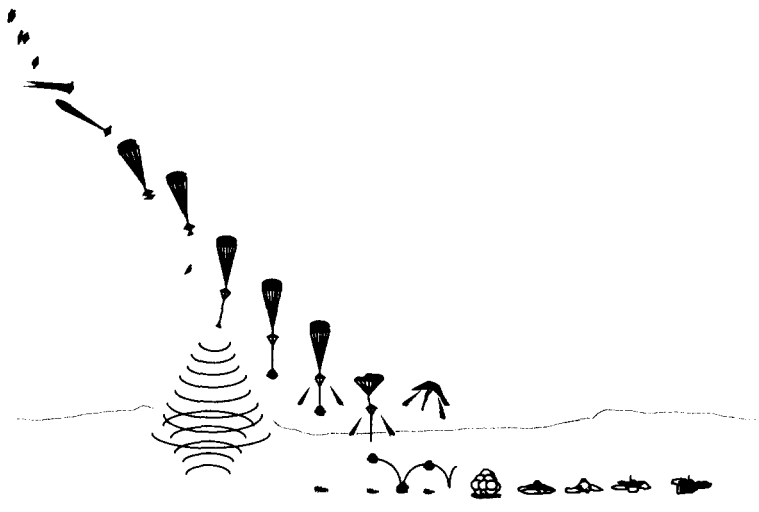

Figure 1. MER EDL Sequence

2 LANDING LOAD CHARACTERIZATION

2.1 Airbag drop testing

Beginning with the MPF mission in 1995 JPL, in collaboration with the airbag system manufacturer ILC Dover Inc., has performed an extensive series of drop tests on full-scale prototype airbag systems. One of the principle objectives for these series of tests is to determine the frequency and magnitude of the landing excitation for an airbag landing system operating under Martian ambient conditions. This drop testing has taken place at NASA Glenn Research Center's Plum Brook Station in the Space Power Facility (SPF), the world's largest space environmental test chamber.

The test configuration consists of an engineering model airbag system attached in flight-like fashion to a full-scale engineering unit lander. The lander is instrumented with accelerometers to record its kinematic motion; additionally, for some drops, the tendons connecting the airbags to the lander were instrumented with load cells to measure the inline tendon forces. All data is recorded on a portable data acquisition system mounted inside the moving lander. The combined airbag/lander assembly is suspended from the top of the SPF chamber and impacted onto an inclined platform with a representative Martian rock field to simulate various landing conditions. All drops take place at pressures of approximately 5 torr, the Martian ambient atmospheric conditions. The drop test setup with is shown in Figure 2.

Figure 2. Airbag Drop Test Setup in SPF

2.2 *Kinematic analysis*

The drop test lander, cocooned inside the suspended airbag system shown in Fig. 2, was instrumented with accelerometers to measure the kinematic response of the test article during impact. In the inertial frame of reference, the position vector of the ith accelerometer ρ_i is related to the position vector of the center of mass of the airbag-lander combination $\mathbf{R}_c$ by

$$\rho_i = \mathbf{R}_c + \mathbf{r}_i, \tag{1}$$

where $\mathbf{r}_i$, is the relative position vector of the ith accelerometer with respect to the center of mass in the body frame of reference. For rigid body rotation, Eq. (1) can be differentiated to obtain the well-known equations

$$\dot{\rho}_i = \dot{\mathbf{R}}_c + \omega \times \mathbf{r}_i \tag{2}$$

and

$$\ddot{\rho}_i = \ddot{\mathbf{R}}_c + \alpha \times \mathbf{r}_i + \omega \times \omega \times \mathbf{r}_i \tag{3}$$

for the velocity and acceleration, respectively, at the ith accelerometer position. For a sufficient set of distributed measurements $\ddot{\rho}_i(t), \alpha(t), \omega(t)$, and $\ddot{\mathbf{R}}_c(t)$ can be analytically reconstructed (Thoma, 2001). A representative plot of the magnitude of the lander-airbag system impact acceleration $|\mathbf{R}_c(t)|$ appears in Fig. 3.

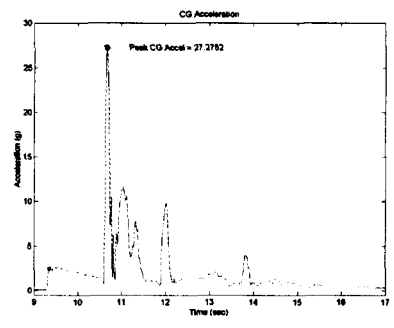

Figure 3. Representative acceleration time history at the center of mass of the lander-airbag system.

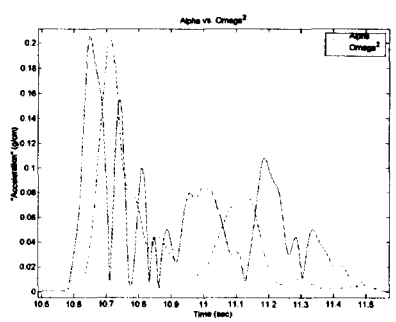

Figure 4. Representative angular acceleration and angular velocity time histories of the lander-airbag system.

Likewise, a representative overlay plot of the magnitudes of the tangential acceleration $|\alpha(t)|$ and the centripetal acceleration $|\omega^2(t)|$—both normalized by the center of mass offset $\mathbf{r}$—appears in Fig. 4 (Thoma, 2001). Note that in comparing Fig. 3 and 4, it is clear that the translational, tangential, and centripetal components of acceleration reach their maxima at different times. This has important implications for deriving a landing load specification.

2.3 *Landing loads specification*

The landing load and its corresponding test specification is expressed in terms of the maximum expected flight environment, or the flight limit load (FLL). The aforementioned time phasing between the various load components becomes an important consideration in determining the overall FLL specification. Since it is very desirable from an engineering perspective to provide a time independent FLL, a methodology must be developed for combining and enveloping the various load components.

2.3.1 Landing loads at the center of mass

The maximum of the translational component of acceleration $\ddot{\mathbf{R}}_c(t)$ determines the FLL at the system center of mass (FLL_{cm}). The significant body of kinematic data from airbag drop testing can be used to statistically derive this value. If the drop test data is normalized to take into account variations in impact kinetic energy and operating pressure as the airbag design has evolved, a collection of the maximum accelerations $\ddot{\mathbf{R}}_{c\,max}$ at the center of mass yields the data set shown in Tab. 1 (Scharton, Adams, presentation, 2002).

Table 1. Peak g loads for drop test data set

Drop	$\ddot{\mathbf{R}}_{c\,max}$ (g)	Drop	$\ddot{\mathbf{R}}_{c\,max}$ (g)
1	10.5	12	14.0
2	11.1	13	15.3
3	11.4	14	18.5
4	20.2	15	16.1
5	12.0	**Statistics**	
6	19.5	Max	20.2
7	19.3	Min	10.5
8	16.1	Mean (μ)	15.2
9	13.0	Sigma (σ)	3.3

If the FLL_{cm} is defined as the 95th percentile load level with 50 percent confidence, then assuming an underlying normal distribution for the μ and σ given in Tab. 1 yields

$$FLL_{cm} = \mu + z_{95/50}\sigma, \tag{4}$$

For $z_{95/50} = 1.68$, Eq. 4 yields a FLL_{cm} of 21 g. This level can be further validated in a more qualitative fashion by utilizing engineering judgement to apply a load uncertainty factor (LUF) to the most representative test case to capture the effects of incomplete analytic simulations or variations in test conditions. Choosing a LUF of 1.15 X for the 18.5 g value from Drop 14— deemed to be the most representative test case—also yields a FLL_{cm} of approximately 21 g.

2.3.2 *Landing loads away from the center of mass*

The maximum of the translational component of acceleration $\ddot{\mathbf{R}}_c(t)$ determines FLL_{cm}; this maximum in conjunction with the maximum of a combination of the tangential acceleration $\mathbf{r}\alpha(t)$ and the centripetal acceleration $\mathbf{r}\omega^2(t)$ determines the FLL for objects not at the system's center of mass. The previously discussed kinematic data can also be used to reconstruct the tangential acceleration $\mathbf{r}\alpha(t)$ and the centripetal acceleration $\mathbf{r}\omega^2(t)$.

Ideally, one could precisely determine the translational and rotational loads at an arbitrary point away from the center of mass using Eq. (3). Generally speaking, this approach is impractical: without the detailed position knowledge to perform the vector analysis implicit in Eq. (3), one cannot solve that equation to develop a unique FLL for each point on the lander body. A more pragmatic engineering approach is to bound the rotational components of acceleration at specified distances from the center of mass to develop bracketed tiers of FLLs. Several options for combining the rotational components to generate the FLLs present themselves:

- algebraically add the acceleration at the center of mass to the maximum tangential acceleration plus the maximum centripetal acceleration; i.e.

$$|\ddot{\rho}|_r^{max} = |\ddot{\mathbf{R}}|_c^{max} + |\alpha\mathbf{r}|^{max} + |\omega^2\mathbf{r}|^{max} \tag{5a}$$

- algebraically add the acceleration at the center of mass to the root of the sum of the squares (RSS) of the angular and centripetal accelerations; i.e.

$$|\ddot{\rho}|_r^{max} = |\ddot{\mathbf{R}}|_c^{max} + \sqrt{|\alpha|^2 + |\omega^2|^2}^{\,max} \tag{5b}$$

- algebraically add the acceleration at the center of mass to the maximum tangential acceleration.

$$|\ddot{\rho}|_r^{max} = |\ddot{\mathbf{R}}|_c^{max} + |\alpha\mathbf{r}|^{max} \tag{5c}$$

The plots in Fig. 5 (Adams, 2002) are useful in helping to choose the most appropriate loads combi-

nation methodology. A comparison of the upper and lower plots in Fig. 5 indicates that for this system, the tangential acceleration peak tends to precede the center of mass and centripetal acceleration peaks. For that reason, generating FLLs according to Eq.'s (5a, 5b) was deemed overly conservative. Consequently, the only question remaining in using Eq. (5c) is to decide the most appropriate point in the time history to select $|\alpha|^{max}$. Because there is no restriction on the lander orientation at impact, and because the time phasing between $|\alpha|$ and $|\ddot{\mathbf{R}}|_c^{max}$ appears variable, $|\alpha|^{max}$ was conservatively chosen as its absolute maximum over the entire time record.

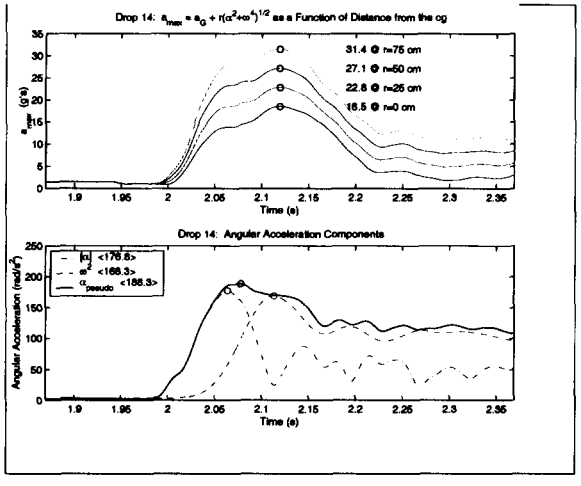

Figure 5. Comparison of rotational accelerations

The maximum angular acceleration observed at any time during Drops 12-15 was $|\alpha|^{max}$=180 rad/s^2, which, after applying a LUF of 1.15 X, yields a peak value of $|\alpha|^{max}_{LUF}$ = 207 rad/s^2 = 0.21 g/cm. Although this value is conservative and ignores any time phasing effects, it is still 8% lower than the angular acceleration measured at the time of $|\ddot{\mathbf{R}}|_c^{max}$ for Drop 4.

2.4 *Flight Limit Loads*

Eq. (5c), in conjunction with the data from Tab. 1 and the results of the previous section, can now be used to generate the FLLs as a function of the offset from the center of mass of the lander-airbag system. These results are summarized in Tab. 2 and 3 below.

Table 2. Flight limit landing loads

Distance from center of mass (cm)	FLL (g's)	FLL with LUF (1.15 X) (g's)
r = 0	18.5	21.2
r = 25	22.8	26.2
r = 50	27.1	31.2
r = 75	31.4	36.1

Table 3. Representative statistics from drops 12–15

		Max	Min	Mean
$\lvert\ddot{\mathbf{R}}\rvert_c$	(g)	18.5	13.5	16.1
$\lvert\alpha\rvert$	(1/s^2)	180	132	162
$\lvert\omega\rvert^2$	(1/s^2)	196	115	152
$\sqrt{\lvert\alpha\rvert^2 + \lvert\omega^2\rvert^2}$	(1/s^2)	216	135	178

3 TEST IMPLEMENTATION

The qualification of MER equipment to landing loads can be considered as having two complementary aspects: a structural testing aspect and an environmental testing aspect. Both approaches derive test levels based on the appropriate margin applied to the FLL. However, a structural testing approach usually has as its primary objective qualifying primary structure by generating *local* loads—typically with the test article in a static test tower—at key equipment interfaces. On the other hand, an environmental test approach usually has as its primary objective qualifying electromechanical equipment and secondary structure by generating *global* loads—typically with the test article on an electrodynamic shaker—measured at either the input to the test article or at its center of mass. By combining loads, modal, and environmental tests into a sequence of tests using a single shaker-based test setup, considerable efficiencies in handling, cost, and schedule may be achieved. (Vujcich, Scharton, 1999) These benefits, however, must be carefully balanced against the drawbacks inherent in dynamically simulating a quasi-static event.

3.1 *Landing load test strategies*

The traditional technique for qualifying a structure to a static load is to perform pull testing in a static test tower or to perform centrifuge testing. As just mentioned, in an effort to minimize the resources intrinsic to implementing these approaches, this paper will outline a technique for simulating a quasi-static load using an electrodynamic shaker. In this technique, a low frequency sine wave excitation—either a multi-cycle sine ramp or a half-sine pulse with a negative pre- and post-pulse—are input to the test article. Force gages at the shaker-test article interface measure the response, thereby determining the acceleration of the test article at its center of mass. Additionally, accelerometers at key test article locations are used to measure other critical hardware responses. To properly implement this technique, one must be cognizant of not only the magnitude but also of the frequency content of the FLLs.

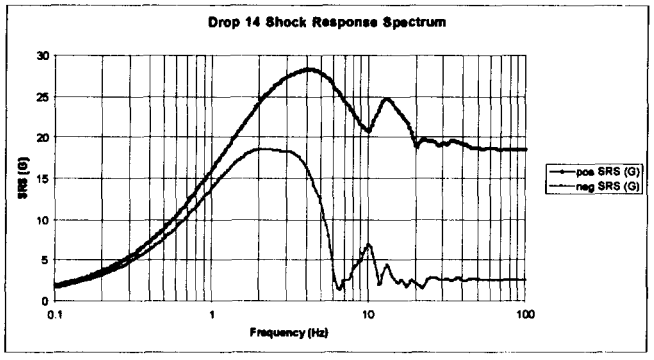

Figure 6. Representative SRS for the landing load excitation

The frequency content of the true landing event can be determined by taking the shock response spectrum (SRS) of the acceleration time history of the center of mass $\ddot{\mathbf{R}}_c(t)$as derived from the drop test kinematic data. A representative SRS from Drop 14 is shown in Fig. 6 (Adams, email, 2002). It is clear from the figure that the landing excitation is a transient event with a main energy lobe at 4 Hz and a secondary lobe at approximately 11 Hz.

It is currently planned to test the MER Rover on the base petal of the MER lander as shown in the configuration drawing displayed Fig. 7. A preliminary finite element analysis (FEA) indicates that the test article in this configuration has a fundamental axial mode at approximately 35 Hz and a fundamental lateral mode at approximately 46 Hz. Since the excitation frequency lies considerably below (more than 1 octave) the fundamental modes of the equipment, there will be minimal dynamic coupling; consequently, the landing load may be effectively treated as a quasi-static load.

Figure 7. Rover - base petal test configuation

Unfortunately, inherent equipment limitations prevent most electrodynamic shakers from generating high g loads at very at low frequencies. This effect occurs because the sinusoidal motion of the shaker table is mechanically limited in stroke, velocity, and force output. This effect is illustrated in Fig. 8. From Fig. 8, it would appear that test equipment limitations preclude reproducing an approximately 30 g landing load excitation with the proper frequency content. Strictly speaking, this true. However, if one realizes that a dynamic excitation applied sufficiently below the fundamental frequencies of a test article is nearly equivalent to a quasi-static

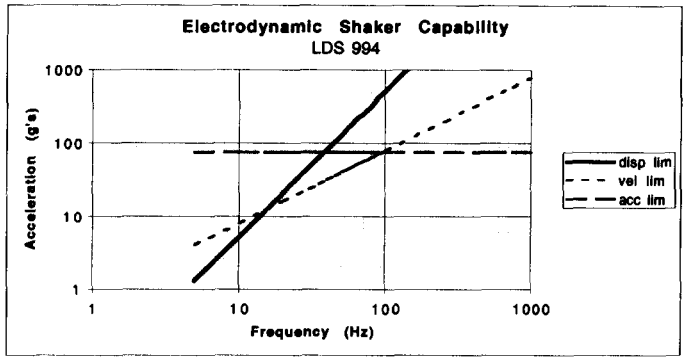

Figure 8. Shaker Capability

excitation of the same magnitude, testing to higher g loads on a shaker becomes realizable. In particular, the JPL shaker is capable of producing a 30 g load at frequencies greater than or equal to approximately 20 Hz, an adequate separation (at least one octave) from the fundamental modes of this test article. What remains is to optimize the excitation waveform to produce the desired excitation and responses.

3.2 *Candidate excitation waveforms*

Various types of transient waveforms may be used for quasi-static loads testing on a shaker. A sine burst, consisting of four cycles of ramp-up, seven cycles at full level, and four cycles of ramp down, was used at Ball Aerospace Corporation's Boulder, CO test facility to test the QuikSCAT spacecraft. (Vujcich, Scharton, 1999) A single half-sine "pulse" was used at IAGB's Munich, GR test facility to test the GRACE spacecraft. A sine burst, consisting of only three cycles of ramp-up, was used at JPL to test the HESSI spacecraft.

All three of these tests were conducted in the "open loop" mode, which means that when the operator hits the button, the pulses are applied to the test item, and there is no way to interrupt them if things aren't right. There was some experimentation with closed loop control in the QuikSCAT pretesting with a mass simulator, but the time constant of the control loop was comparable to the duration of the burst, and the results showed considerable variability from test to test. In the case of the GRACE tests, it was necessary to use the half-sine pulse, which is much too fast to control in real time, in order to limit the loading in the negative direction, which would have caused damage to a joint with insufficient preload. In the case of the HESSI test, there was a shaker malfunction, which resulted in significant damage to the spacecraft, which is shown in Fig. 9. The cause of the HESSI over-test was stiction in the shaker slip table during the shaker self check. (The self-check is a low-level random pretest, which the shaker computer conducts before the pulse test in order to get a transfer function between the specified acceleration and the required input

voltage.) Needless to say, there are now many safety procedures in place at JPL to avoid a reoccurrence of the HESSI incident.

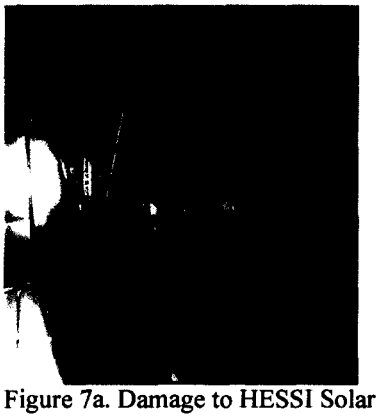

Figure 7a. Damage to HESSI Solar Array

Figure 9b. Damage to HESSI Support Ring

Based on this experience, the two candidate waveforms appearing most viable for the MER quasi-static landing excitation are the half-sine pulse and the sine ramp. Plots of these two waveforms are shown in Fig. 10 and 11, respectively.

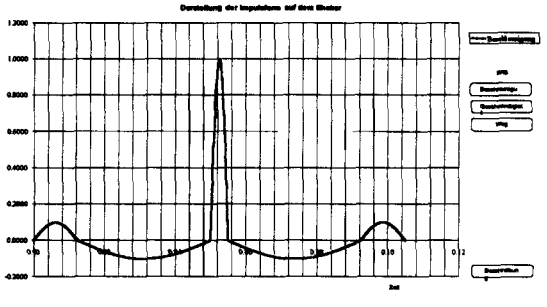

Figure 10. The half-sine pulse

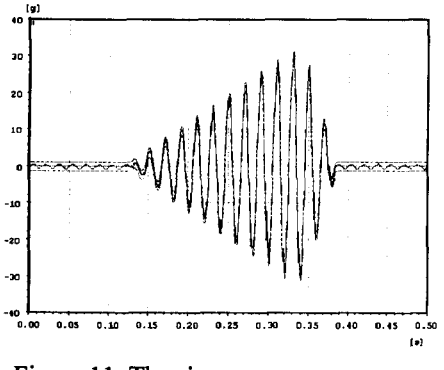

Figure 11. The sine ramp

After some experimentation on the shaker, the sine ramp was deemed preferable over the half-sine pulse for implementing a quasi-static test load. The sine ramp offers the advantages of (1) containing less high frequency content in the pre- and post-pulse than does the half-sine pulse and (2), having a peak-limiting capability to provide for an for automatic shutdown capability in the event of an accidental overtest. These advantages are slightly offset by the fact that the sine ramp does introduce more cycles into the test article than does the half-sine pulse. Another important criterion for waveform selection is the comparative response of the test article.

3.3 *Equipment responses to the candidate waveforms*

Even though the frequency of the shaker-based input excitation is designed to lie one or more octaves below the fundamental frequency of the test article, some dynamic amplification will still occur. Amplification results because both input waveforms contain some high frequency content, and because the transmissibility function at a one octave band frequency separation is still greater than unity. Because the response is different at the various positions on the structure and it is, in general, impossible to mount an accelerometer at the center-of gravity of a flexible structure, force gages mounted between the structure and shaker are used to measure the acceleration response of the test item center-of-gravity. (The acceleration of the center-of-gravity is of course the total external force divided by the total mass, by Newton's 2nd law.)

To better quantify the aforementioned response variation, a FEA has been performed to analytically predict equipment responses at key test article locations. For this analysis, comparative responses were tabulated for both a 20 Hz sine ramp and a 20 ms half-sine pulse input excitation. These results are summarized in Tab. 4.

Table 4. Comparison of FEA responses of appendages with design loads (input adjusted to obtain 25 g response at the CG)

transient sign	location	x-acc (g's)	y-acc (g's)	z-acc (g's)	Design Loads (g
sine ramp	solar panel	42.3	41.7	29.8	49 (landing load)
	n 21543, Battery Assembly	24.5	26.3	24.7	40 (landing load)
	n25000, Instrument Arm	25.0	25.3	26.9	42 (landing load)
	n26282, Mini-Tes	26.0	25.7	27.0	39.7 (landing load)
	n 26283, REM	25.0	25.5	24.9	40.2 (landing load)
	n 26284, LGA	29.3	27.8	24.8	60 (MAC)
	n 26286, HGA	38.1	27.4	24.7	43.1 (landing load)
	n 31001, UHF Antenna	29.2	39.1	19.3	100 (MAC)
	base pedal input	24.0	23.6	24.5	
half sine	solar panel	48.8	52.3	41.9	49 (landing load)
	n 21543, Battery Assembly	25.8	29.0	25.1	40 (landing load)
	n25000, Instrument Arm	24.1	30.2	30.6	42 (landing load)
	n26282, Mini-Tes	26.2	27.2	30.6	39.7 (landing load)
	n 26283, REM	28.3	29.4	26.1	40.2 (landing load)
	n 26284, LGA	30.0	31.0	25.1	60 (MAC)
	n 26286, HGA	43.9	30.3	24.8	43.1 (landing load)
	n 31001, UHF Antenna	34.0	47.2	23.1	100 (MAC)
	base pedal input	21.8	20.3	20.2	

It is interesting to note that according to this analysis, dynamic amplifications in excess of 2.0 X occur even at octave band frequency separations. The data from Tab. 4 indicate that, on the whole, the sine ramp waveform appears to overtest the equipment less than does the half-sine pulse.

3.4 *Extrapolation of Vibration Test Data*

A variety of sophisticated analytical and experimental techniques are available for identifying the vibration behavior of spacecraft and for correlating analytical models with ground test and flight data. However, few techniques exist for extrapolating the knowledge gained from these correlations of analysis and test of existing hardware to new configurations. The object of a current R&D task at JPL is to develop methods for using FEA to extrapolate the results of vibration tests to new designs, not yet built or tested.

One method under development is analogous to the modal mass acceleration curve (MMAC) currently used at JPL and other aerospace organizations to characterize the dynamic excitation of spacecraft by different launch vehicles. The MMAC is a semi-empirical curve of the maximum acceleration of each vibration mode on the ordinate versus the effective mass of that mode plotted on the abscissa. FEA is used to apply the MMAC predictions to new structural configurations with different geometries and equipment. Another method under investigation involves extrapolating ratios of the measured to calculated values of key structural parameters, such as natural frequency, damping, and effective mass, to the new design. A third method involves extrapolating the tuning steps used to reconcile the FEA model and test data for the existing configuration to the FEA model of the new design.

These differing candidate extrapolation techniques will be applied and evaluated using the vibration test data generated in the MER program. The MER program includes vibration tests of both a development test model (DTM) and flight version of the rover-base petal configuration. These two configurations differ primarily in that the DTM has mass or dynamic simulators for many of the appendages. In addition, an exploratory test using the DTM rover-base petal configuration for the 1995 MPF has been conducted to help plan the MER test program. The FEA of these three Rover-base petal configurations will be used to extrapolate the results of the Pathfinder DTM test to the MER DTM test, and then again to extrapolate the results of the MER DTM test to the MER flight hardware test. The different extrapolation methods will then be evaluated using the final test data.

4 CONCLUDING REMARKS

In this paper, a novel approach for utilizing sine-burst excitations from an electrodynamic shaker to generate quasi-static loads is described. In this technique, a low frequency, multi-cycle sine ramp waveform is input to the test article. Force gages at the shaker-test article interface measure the response, thereby determining the acceleration of the test article at its center of mass. Additionally, accelerometers at key test article locations are used to measure other critical hardware responses and calibrate the input excitation.

These data can be subsequently incorporated into a finite element model to predict responses at other test article locations, or be extrapolated to predict responses for other similar structures. Various techniques for using FEA to extrapolate the results of vibration tests to new designs not yet built or tested are now being investigated. Vibration test data now being generated in the ongoing program for qualifying MER equipment to Martian landing loads will be used to evaluate the various extrapolation techniques.

Finally, by combining loads, modal, and environmental tests into a sequence of tests using a single shaker-based test setup, considerable efficiencies in handling, cost, and schedule may be achieved. While the goals of static and environmental testing are closely related, reconciling test levels to accomplish the objectives of both may involve some compromises since a dynamic event is being used to generate a quasi-static load.

ACKNOWLEDGEMENTS

The work described in this paper was carried out by the Jet Propulsion Laboratory, California Institute of Technology, under a contract with the National Aeronautics and Space Administration. The authors wish to express their appreciation to Doug Adams and Tim Werner of JPL for their invaluable assistance during this project.

REFERENCES

Adams, D.S. 2002. MER Airbag Landing Loads and Analysis Update 2. *Jet Propulsion Laboratory* (Pasadena, CA), Internal Memorandum 352F:02:002:DSA.

Thoma, Ben. 2001. Mars Exploration Rover Airbag Landing Loads and Analysis. *Jet Propulsion Laboratory* (Pasadena, CA), Internal Memorandum 352D:01:021:BLT.

Vujcich, M. and T. Scharton. 1999. Combined dynamic testing of the QuikSCAT spacecraft. Presented at the *SAE/AIAA World Aviation Conference* (October), San Francisco.